remote sensing

MDPI

Article

Vegetation Greening and Its Response to a Warmer and Wetter Climate in the Yellow River Basin from 2000 to 2020

Yan Bai [1,2,*], Yunqiang Zhu [1,2], Yingzhen Liu [3] and Shu Wang [1,2]

[1] State Key Laboratory of Resources and Environmental Information System, Institute of Geographic Sciences and Natural Resources Research, Chinese Academy of Sciences, Beijing 100101, China; zhuyq@igsnrr.ac.cn (Y.Z.); wangshu@igsnrr.ac.cn (S.W.)
[2] Jiangsu Center for Collaborative Innovation in Geographical Information Resource Development and Application, Nanjing 210023, China
[3] State Key Laboratory of Geo-Information Engineering, Xi'an 710054, China; liufan@126.com
* Correspondence: baiy@lreis.ac.cn

Abstract: Vegetation greening is time-dependent and region-specific. The uncertainty of vegetation greening under global warming has been highlighted. Thus, it is crucial to investigate vegetation greening and its response to climate change at the regional scale. The Yellow River Basin (YRB) is a vital ecological barrier in China with high ecological vulnerability and climatic sensitivity. The relationship between vegetation greening and climate change in the YRB and the relative contribution of climate change remain to be explored. Using the Enhanced Vegetation Index (EVI) and meteorological observation data, the spatiotemporal patterns of vegetation greening across the YRB in response to climate change at the basin and vegetation sub-regional scales from 2000 to 2020 were analyzed. The impact of human activities on regional greening was further quantified. Results showed that approximately 92% of the basin had experienced greening, at average annual and growing season rates of 0.0024 and 0.0034 year^{-1}, respectively. Greening was particularly prominent in the central and eastern YRB. Browning was more prevalent in urban areas with a high intensity of human activities, occupying less than 6.3% of the total basin, but this proportion increased significantly at seasonal scales, especially in spring. Regional greening was positively correlated with the overall warmer and wetter climate, and the partial correlation coefficients between EVI and precipitation were higher than those between EVI and temperature. However, this response varied among different seasonal scales and vegetation sub-regions. The combined effects of climate change and human activities were conducive to vegetation greening in 84.5% of the YRB during the growing season, while human activities had a stronger impact than climate change. The relative contributions of human activities to greening and browning were 65.15% and 70.30%, respectively, mainly due to the promotion of ecological rehabilitation programs and the inhibition of urbanization and construction projects.

Keywords: EVI; vegetation sub-region; climate change; relative contribution; Yellow River Basin

Citation: Bai, Y.; Zhu, Y.; Liu, Y.; Wang, S. Vegetation Greening and Its Response to a Warmer and Wetter Climate in the Yellow River Basin from 2000 to 2020. *Remote Sens.* **2024**, *16*, 790. https://doi.org/10.3390/rs16050790

Academic Editor: Liming Zhou

Received: 13 January 2024
Revised: 18 February 2024
Accepted: 19 February 2024
Published: 24 February 2024

1. Introduction

Vegetation, an irreplaceable ingredient of the terrestrial ecosystem, considerably modulates the land–atmosphere exchange of water, energy, and carbon cycles [1]. Substantial evidence suggests that climate change is rapidly altering vegetation dynamics owing to biophysical plant responses such as respiration, photosynthesis, and evapotranspiration [2]. Meanwhile, vegetation activity provides major feedback on climate change [3]. For example, enhanced vegetation growth and extended growing seasons may result in a cooling effect through increased evapotranspiration or a warming effect through decreased surface albedo [4,5]. Vegetation–climate interactions are critical to the sustainability of the ecosystem and are particularly important for the implementation of ecological conservation and

restoration measures. Therefore, it is necessary to understand the spatiotemporal trends in vegetation variations and its response to climate change.

Satellite observations [6], vegetation inventories [7], and ecosystem models [8] have consistently reported global greening since the 1980s. Greening is substantial in the northern temperate and high-latitude regions [9] and is notably prominent in regions of afforestation and agricultural intensification, such as China and India [10]. However, the observed greening is not universal due to differences in natural environment and socioeconomic development. Some regions, especially those in northern Eurasia [11], the African Sahel-Sudano-Guinean region [12], and the Congo Basin [13], have experienced largely expanded browning since the late 1990s, suggesting that vegetation dynamics in many regions may have been reversed from the greening [14]. The spatiotemporal heterogeneity of vegetation greening has been confirmed across seasons and regions, as well as for land cover types [15]. Additionally, several negative effects, such as insufficient cross-calibration of sensors, sensor degradation, and atmospheric contamination of sensor signals [16], can result in inconsistencies of the estimated vegetation greening based on different satellite data [9] and thus lead to inconsistent responses of vegetation greening to climate change [17]. Thus, continuous investigation on vegetation greening and its intrinsic driving forces based on multi-source data is imperative.

Variations in vegetation greening have been widely attributed to the CO_2 fertilization effect, climate change, and land use management [10]. Increasing concentrations of atmospheric CO_2 is considered to be the major driver of global greening [6]. However, Norby et al. [18] suggested that the buffering capacity of vegetation greening is limited under climate warming because of vegetation photosynthesis saturation caused by the CO_2 fertilization effect. Climate change is a significant driver contributing to the greening trend in over 28.4% of global vegetated areas; however, this impact varies regionally [6]. For example, warming decreases the photosynthesis activity of vegetation in tropical regions where the growing season air temperature comes close to the optimum temperature for vegetation growth [19]. Conversely, warming notably promotes vegetation greening in northern high latitudes, owing to the eased climatic constraints in cold regions [20]. Separating warming from water relations in terms of influence on vegetation greening is challenging. Considering the increased demand for evaporation and decreased soil water availability, the negative impact of warming and water stress (such as drought) on vegetation greening has been observed in many regions, particularly in the tropics, including Amazonia [21], temperate and boreal Eurasia [11], and the Congo Basin [13]. Moreover, the magnitude of drought trends fluctuated as the time scale expanded [22], and the response of vegetation growth to meteorological drought varied evidently across multi-scales and vegetation categories [23]. Furthermore, accumulating evidence suggests that the response of vegetation to temperature has weakened in northern temperate ecosystems over the last three to four decades [20]. However, the cause of this phenomenon remains unclear. Recently, a stalling or a reversal trend of greening was recognized, highly pronounced in the mid–low latitudes of the Northern Hemisphere after the late 1990s [14]. This further imposes large complexities and uncertainties on the response of vegetation greening to rapid environmental changes in the context of global warming, especially in northern temperate regions.

The Yellow River Basin (YRB) is a vital ecological barrier in China, and it is a typical transitional zone between monsoon and continental climates. Considering its climatic sensitivity and ecological vulnerability, the YRB offers an opportunity for the ongoing examination of vegetation greening and its response to climate change at a sub-regional scale within northern temperate regions. Although general vegetation greening across the YRB has been reported [24], a recent study indicated weakened greening in the basin, which is anticipated to continue in urban and surrounding areas [25]. However, understanding of the response and driving mechanism of vegetation greening in different ecosystem regions across the YRB remains limited, with few studies quantifying the relative contribution of driving factors, such as climate change and human activities, to vegetation greening.

Moreover, previous studies on vegetation dynamics in the YRB have primarily relied on low-resolution satellite-derived Normalized Difference Vegetation Index (NDVI) data (8 km, 1 km, or 500 m) [24,26,27], with a notable absence of studies applying the nearest and latest time series of other vegetation index data at higher resolutions.

This study aimed to investigate the spatial–temporal trends in vegetation greening and climate change, as captured by the Enhanced Vegetation Index (EVI) and meteorological observation data, and explore the response and driving relationship between them across the YRB from 2000 to 2020. The impacts of human activities on vegetation greening were also quantified. Considering that vegetation dynamics are highly dependent on period and region, this study focused on gaining a deeper understanding of vegetation greening and their responses to climatic change across varying spatial (basin and vegetation sub-regions) and temporal (annual, growing season, and seasonal) scales. The following three key issues were explored: (i) the spatiotemporal patterns of the EVI greening and climatic change in the YRB, (ii) the relationships between EVI greening and climatic change among different vegetation types, and (iii) the relative contributions of two main driving factors (i.e., climate change and human activity) to the observed EVI greening.

2. Materials and Methods

2.1. Study Area

The YRB (95°53′–119°05′E, 32°10′–41°50′N) crosses nine provinces (or autonomous regions) in northern China, including Qinghai, Sichuan, Gansu, Ningxia, Inner Mongolia, Shaanxi, Shanxi, Henan, and Shandong, with an area of 7.95×10^5 km^2 (Figure 1a). The topography and landforms in the YRB differ significantly. The terrain of the basin is high in the west, dominated by a series of mountains at an average altitude over 4000 m, and is low in the east, largely covered by alluvial plain at elevations below 100 m. The central region is mainly a loess landform with severe soil erosion. As a semi-arid and semi-humid climate transition zone with uneven spatial distributions of temperature and precipitation, there are five sub-regions with various vegetation types in the YRB, including: (I) warm temperate deciduous broad-leaved forest, (II) subtropical evergreen broad-leaved forest, (III) temperate grassland, (IV) temperate desert, and (V) alpine vegetation in the Qinghai–Tibet Plateau. The spatial distribution of the growing season EVI increases from northwest to southeast across the YRB (Figure 1b). Sub-regions I and II, primarily with forests and croplands, have high EVI, whereas the other three sub-regions dominated with typical grasslands, desert grasslands, and steppe deserts exhibit relatively low EVI, especially in the Ordos Plateau, Longzhong Plateau, and the source region of the Yellow River.

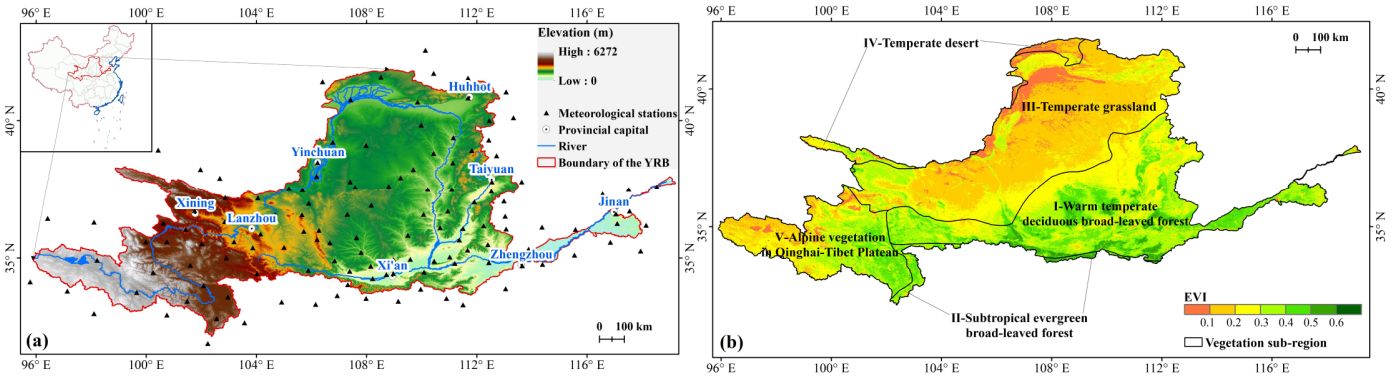

Figure 1. (**a**) Geographic location, elevation, spatial distribution of meteorological stations, and (**b**) vegetation sub-regions with growing season averaged EVI of the YRB.

2.2. Data Sources

Vegetation information was obtained from the 16-day and 250 m EVI product (MOD13Q1, C6, HDF format) of the Moderate Resolution Imaging Spectroradiometer (MODIS) on board

the Aqua and Terra from 2000 to 2020. These data are available from the NASA Earth Observing System Data and Information System (https://earthdata.nasa.gov/ (accessed on 30 August 2023 to 12 September 2023)). The missing MODIS EVI data for the first 49 days of 2000 were substituted with average data for the same period from 2001 to 2020, and a maximum value composite method was applied to generate the monthly EVI data. Subsequently, the average EVI for the annual, growing season (April to October), spring (March to May), summer (June to August), and autumn (September to November) were calculated for further analysis.

Daily climate data (originally TXT format), including temperature and precipitation during 1991–2020, were collected from 133 meteorological stations in the YRB at the China Meteorological Data Service Center (http://data.cma.cn/ (accessed on 21 September 2023)) (Figure 1a). The gridded monthly mean temperature (TMP, °C) and accumulated precipitation (PRE, mm) data with a spatial resolution of 250 m were interpolated by Anusplin 4.4 software, using the local thin-plate spline method, introducing a quadratic model that applies elevation as a covariate for temperature interpolation and a non-covariate quadratic model for precipitation interpolation.

The 30 m elevation data were obtained from the Advanced Spaceborne Thermal Emission and Reflection Radiometer Global Digital Elevation Model (ASTER GEDM, TIFF format), provided by NASA's Land Processes Distributed Active Archive Center (https://lpdaac.usgs.gov/ (accessed on 21 September 2023)). They were resampled to 250 m using the nearest-neighbor method in the interpolation process. Vegetation sub-region data with shapefile format were acquired from the National Earth System Science Data Center of China (NESSDC, http://www.geodata.cn/ (accessed on 21 September 2023)).

2.3. Methods

2.3.1. Trend Analysis

Two nonparametric methods, including the Theil–Sen and Mann–Kendall (M–K), were applied to measure the slope of trends and test their significances in the EVI and climatic variables across the YRB. The Theil–Sen is robust in trend analysis and effectively addresses small outliers and missing data without requiring time-series data to meet serial autocorrelation and normal distribution assumptions [28]. The M–K test is commonly used to detect the significance of time-series trends as a supplement to the Theil–Sen [29]. The Theil–Sen formula is as follows:

$$\beta = Meadian\left(\frac{x_j - x_i}{j - i}\right), \forall j > i \quad (1)$$

where β is the median slope of the time series, and x_i and x_j are the index values of the ith and jth time series, respectively. $\beta > 0$ indicates an increasing trend while $\beta < 0$ indicates a decreasing trend. The significance of time-series trends (represented by p) is measured by the M–K test, and $p < 0.05$ means that the significance level of 95% is passed. The trends of vegetation coverage are classified into the following five categories, according to the results of the M–K test: significant greening ($\beta \geq 0.001$, $p \leq 0.05$), slight greening ($0.0001 \leq \beta < 0.001$, $p > 0.05$), stable or non-vegetated ($-0.0001 \leq \beta < 0.0001$, $p > 0.05$), slight browning ($-0.001 \leq \beta < -0.0001$, $p > 0.05$), and significant browning ($\beta < -0.001$, $p \leq 0.05$).

2.3.2. Partial Correlation Analysis

Partial correlation analysis was conducted to analyze the apparent responses of EVI to temperature and precipitation to eliminate the covariate effects of other factors [30]. Specifically, the partial correlation coefficient (PCC) between EVI and temperature with

precipitation as the control variable, and the PCC between EVI and precipitation while controlling the influence of temperature, are calculated as follows:

$$PCC_{xy,z} = \frac{R_{xy} - R_{xz}R_{yz}}{\sqrt{\left(1 - R_{xz}^2\right)\left(1 - R_{yz}^2\right)}} \quad (2)$$

$$R_{xy} = \frac{\sum_{i=1}^{n}\left[\left(x_i - \overline{x}\right)\left(y_i - \overline{y}\right)\right]}{\sqrt{\sum_{i=1}^{n}\left(x_i - \overline{x}\right)^2}\sqrt{\sum_{i=1}^{n}\left(y_i - \overline{y}\right)^2}} \quad (3)$$

where $PCC_{xy,z}$ is the partial correlation coefficient between the two variables x and y when z is the control variable, R_{xy}, R_{xz}, and R_{yz} are the pairwise correlation between x, y, and z, and $\overline{x}$ and $\overline{y}$ are the average values of these two variables for n years. A t-test is used to estimate the significance of the PCC among EVI, temperature, and precipitation, which are classified into the following four types: significant positive correlation ($PCC_{xy,z} \geq 0$, $p \leq 0.05$), significant negative correlation ($PCC_{xy,z} < 0$, $p \leq 0.05$), positive correlation ($PCC_{xy,z} \geq 0$, $p > 0.05$), and negative correlation ($PCC_{xy,z} < 0$, $p > 0.05$).

2.3.3. Residual Analysis

Residual analysis has been widely used to differentiate human-induced vegetation changes from those driven by climatic factors [31], based on the assumption that climate change and human activities are the main drivers of vegetation variations. Using TMP and PRE data, the predicted value of EVI (EVI_{CC}) was fitted per pixel by employing Multivariate Linear Regression (MLR) to represent the impact of climate change. Then, the difference between the true EVI (EVI_{TRUE}) and the predicted EVI (EVI_{CC}), referred to as the residuals of EVI (EVI_{HA}), was obtained to represent the influence of human activities. The formula is as follows:

$$EVI_{CC} = a \times TMP + b \times PRE + c \quad (4)$$

$$EVI_{HA} = EVI_{TRUE} - EVI_{CC} \quad (5)$$

where a and b are the regression coefficients among EVI and TMP and PRE in the MLR model, respectively; c is a constant. Trend analysis (Equation (1)) was applied to detect the trends in EVI_{CC} and EVI_{HA}. $\beta > 0$ indicates that climate change or human activities can promote vegetation growth; otherwise, climate change or human activities may inhibit vegetation growth. According to the results of the residual analysis, the relative contributions of climate change and human activities, referring to the combined effects of the two drivers rather than the relative contribution of each [32], were quantified, as shown in Table 1.

Table 1. Relative contributions of climate change and human activities to EVI growth.

EVI Trend	$\beta(EVI_{CC})$	$\beta(EVI_{HA})$	Relative Contributions (%)		Explanation
			Climate Change (CC)	Human Activities (HA)	
Greening	>0	>0	$\frac{\beta(EVI_{CC})}{\beta(EVI_{CC})+\beta(EVI_{HA})} \times 100$	$\frac{\beta(EVI_{HA})}{\beta(EVI_{CC})+\beta(EVI_{HA})} \times 100$	Climate change and human activities both promote EVI growth
	>0	<0	100	0	Climate change promotes EVI growth
	<0	>0	0	100	Human activities promote EVI growth
Browning	<0	<0	$\frac{\beta(EVI_{CC})}{\beta(EVI_{CC})+\beta(EVI_{HA})} \times 100$	$\frac{\beta(EVI_{HA})}{\beta(EVI_{CC})+\beta(EVI_{HA})} \times 100$	Climate change and human activities both inhibit EVI growth
	<0	>0	100	0	Climate change inhibits EVI growth
	>0	<0	0	100	Human activities inhibit EVI growth

3. Results

3.1. Vegetation Greening Derived by EVI from 2000 to 2020

3.1.1. Temporal Variations of EVI

The temporal fluctuations in the annual EVI (EVI_{AN}), growing season EVI (EVI_{GS}), and seasonal EVI, including spring EVI (EVI_{SP}), summer EVI (EVI_{SU}), and autumn EVI (EVI_{AU}), for vegetation coverage in the YRB from 2000 to 2020 are presented in Figure 2. At the river basin scale, all five time scales revealed a fluctuating increase in the EVI since 2000, with significant greening observed at rates of 0.0024/year and 0.0034/year ($p < 0.01$) in EVI_{AN} and EVI_{GS}, respectively. Except in autumn, the average EVI peaked in 2018 and notably increased in 2002 and 2012. Among the three seasons, the most significant greening was observed in summer at a rate of 0.0040/year, followed by autumn at a rate of 0.0026/year and spring at the lowest increasing rate of 0.0019/year ($p < 0.05$). These findings strongly suggest significant differences in vegetation greening rates among different seasons.

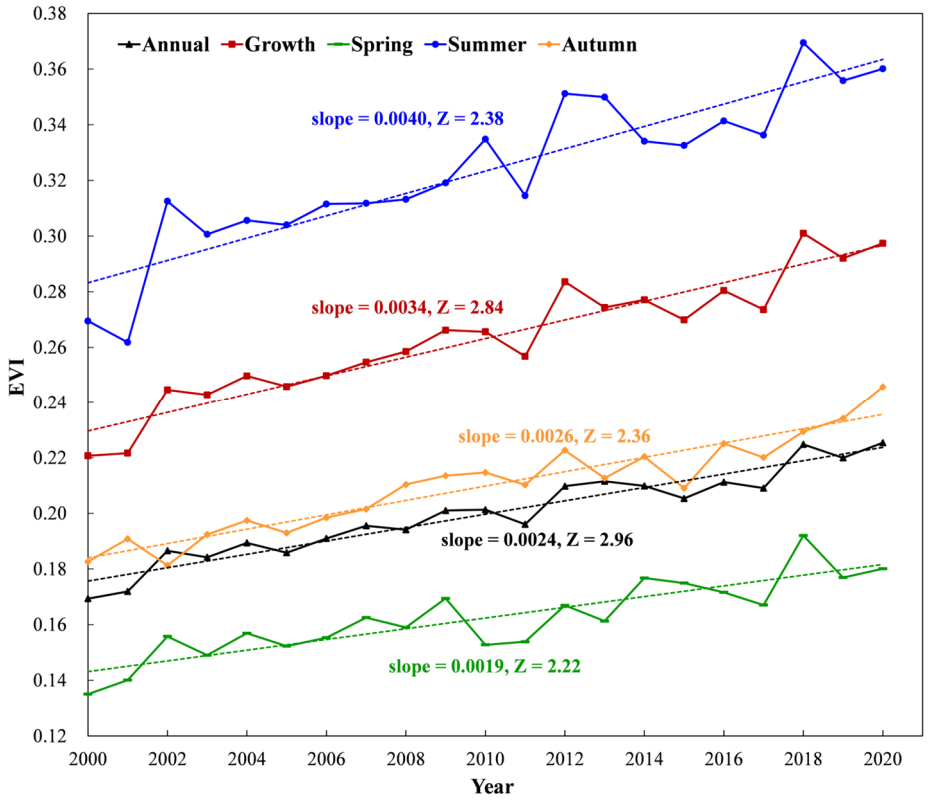

Figure 2. Temporal variations of the annual, growing season, and seasonal averaged EVI in the YRB during 2000–2020.

3.1.2. Spatial Patterns of EVI Greening

More than 75% of the YRB showed significant trends (either greening or browning, $p < 0.05$) in annual and growing season average EVIs over the past 21 years (Figure 3a,b). Specifically, EVI_{AN} and EVI_{GS} increased in 91.92% and 92.68% of the study area, respectively, of which 75.67% and 74.05% showed significant greening, primarily distributed in the middle and eastern regions of the YRB, covering most of the Loess Plateau. Less than 6.30% of the entire basin decreased in EVI_{AN} and EVI_{GS}, of which only 1.40% showed significant browning, mainly clustered in the southern Sichuan–Tibet Plateau and urban areas with a high intensity of human activities, such as the City Belt along the Yellow River in Ningxia with Yinchuan as the center, Taiyuan and surrounding areas, the Guanzhong Plain urban agglomeration centered on Xi'an, and the Central Plains urban agglomeration centered on Zhengzhou. Areas with stable or non-vegetated trends accounted for less than 1.85% and were sporadically distributed in the upper reaches of the YRB. Approximately

64% of the YRB experienced significant greening in the three seasons (63.81% for EVI_{SP}, 63.65% for EVI_{SU}, and 63.61% for EVI_{AU}), but more pixels exhibited slight greening and browning in seasonal EVI than in annual and growing season EVIs (Figure 3c–f). Among all the time ranges, the smallest significant browning was detected in 1.21% of the YRB in autumn. In comparison, the largest browning (11.81%) and stable or non-vegetated trends (2.26%) were found in spring, including 2.85% that exhibited significant browning, which was distributed prominently in the Hetao Plain, as well as the above-mentioned urban expansion areas. In summer, a large area of EVI increased (91.10%), and only a small area showed browning (7.82%); the spatial pattern of the EVI greening was similar to that of the growing season.

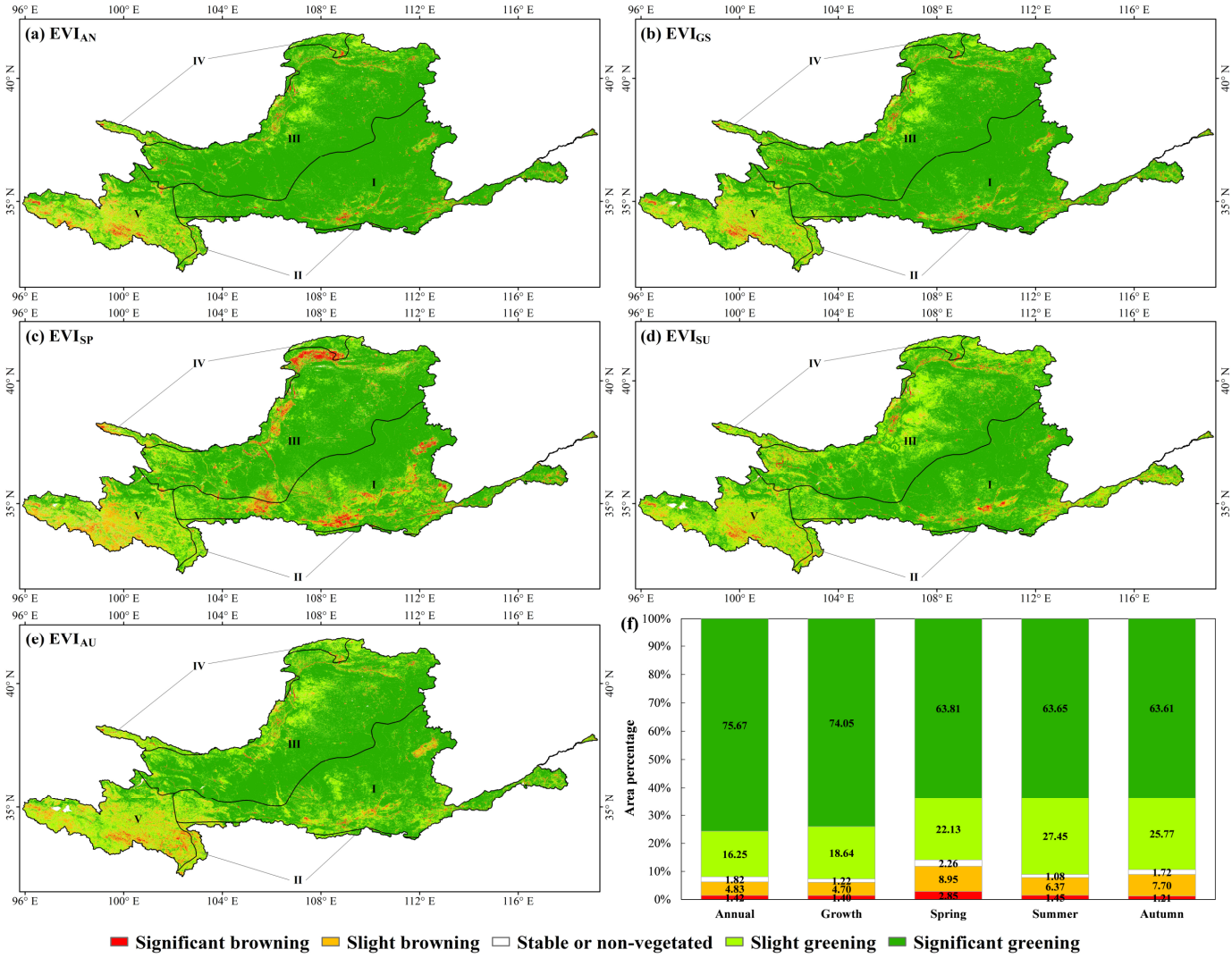

Figure 3. Spatial patterns of (**a**) annual, (**b**) growing season, (**c**) spring, (**d**) summer, and (**e**) autumn EVI variation trends in the YRB from 2000 to 2020; (**f**) the area percentage (%) of variation trends at different time scales.

At the ecosystem scale (Table 2), all vegetation sub-regions showed increasing trends from 2000 to 2020, with the largest rates of increase in summer. Sub-regions I and III exhibited significant greening at all time scales, with increasing rates greater than 0.0032/year ($p < 0.01$) and 0.0014/year, respectively. In addition, sub-region I had the largest area of significant greening, except in spring and autumn. Sub-region V was the only one that exhibited the largest browning at each time scale, especially in autumn, where the browning area accounted for more than 28%. However, the proportion of areas with significant

browning was very small in each sub-region, with the largest significant browning being only 4.52%, which occurred over sub-region IV in spring.

Table 2. EVI variation trends of different vegetation types in the YRB during 2000–2020.

Time Scale	Vegetation Sub-Region	Slope of EVI (β)	Area Percent of Variation Trend (%)				
			Significant Greening	Slight Greening	Stable or Non-Vegetated	Slight Browning	Significant Browning
Annual	I	0.0036 **	87.71	7.95	0.52	2.43	1.39
	II	0.0017 *	57.88	30.54	3.10	7.38	1.10
	III	0.0022 **	83.82	12.21	0.94	2.12	0.91
	IV	0.0008	50.99	34.78	4.76	7.24	2.23
	V	0.0007	33.83	40.48	6.40	16.55	2.73
Growing season	I	0.0049 **	84.75	10.27	0.48	3.06	1.45
	II	0.0024	51.83	35.69	2.46	9.04	0.98
	III	0.0031 **	81.35	14.72	0.65	2.30	0.98
	IV	0.0013	53.23	35.83	3.01	6.00	1.93
	V	0.0012	37.10	42.72	3.89	13.91	2.38
Spring	I	0.0032 *	67.10	20.87	0.92	7.44	3.66
	II	0.002	41.76	47.67	2.55	7.03	0.99
	III	0.0014 **	76.77	14.84	1.50	4.34	2.56
	IV	0.0005	44.41	31.76	5.34	13.97	4.52
	V	0.0005	28.52	39.39	6.69	23.70	1.70
Summer	I	0.0058 **	77.05	16.66	0.49	4.38	1.42
	II	0.0027	43.62	40.13	1.77	12.93	1.54
	III	0.0036 *	67.52	26.47	0.84	4.00	1.17
	IV	0.0016	36.06	50.17	2.99	8.74	2.04
	V	0.0017	30.35	48.95	2.64	15.92	2.13
Autumn	I	0.0034 **	71.80	21.42	0.86	4.84	1.08
	II	0.0013	23.11	48.31	4.00	22.77	1.80
	III	0.0028 **	77.90	17.98	0.85	2.55	0.72
	IV	0.001	34.18	50.22	4.14	9.76	1.70
	V	0.0006	17.39	49.13	5.26	25.62	2.61

* and ** indicate $p < 0.05$ and $p < 0.01$, respectively.

3.2. Climate Change from 1991 to 2020

3.2.1. Interannual Trend of Climatic Variations

Figure 4 indicates that the YRB has experienced a warmer–wetter trend over the past three decades (1991–2020). Temperatures in the YRB across five time ranges all showed significant increasing trends at rates greater than 0.032 °C/year ($p < 0.05$), except for summer (0.030 °C/year, $p = 0.068$). Precipitation exhibited an insignificant increasing trend at rates greater than 0.533 mm/year ($p > 0.05$), except for autumn (1.367 mm/year, $p < 0.05$). As for different vegetation sub-regions of the YRB, temperature exhibited a significant warming trend at all time ranges except for summer temperature in sub-regions I and III, with rates greater than 0.021 °C/year in sub-region I, 0.039 °C/year in sub-region II, 0.027 °C/year in sub-region III, 0.030 °C/year in sub-region IV, and 0.023 °C/year in sub-region V. Precipitation also showed increasing trends in different sub-regions at rates greater than 0.460 mm/year in sub-region I, 1.514 mm/year in sub-region II, 0.539 mm/year in sub-region III, 0.666 mm/year in sub-region IV, and 1.206 mm/year in sub-region V. Meanwhile, across sub-region V, a highly significant warming trend ($p < 0.01$) was detected except in spring, and a significant wetter trend ($p < 0.05$) was observed except in summer. During 1991–2020, temperatures in sub-regions I and III, as well as precipitation in sub-regions I and II, were higher than those in the entire basin. At the river basin scale, the maximum change slope of temperature and the minimum change slope of precipitation both occurred in spring, suggesting that the YRB had the most evident warming tendency but the weakest wetter tendency in spring over the past 30 years (Figure 4c).

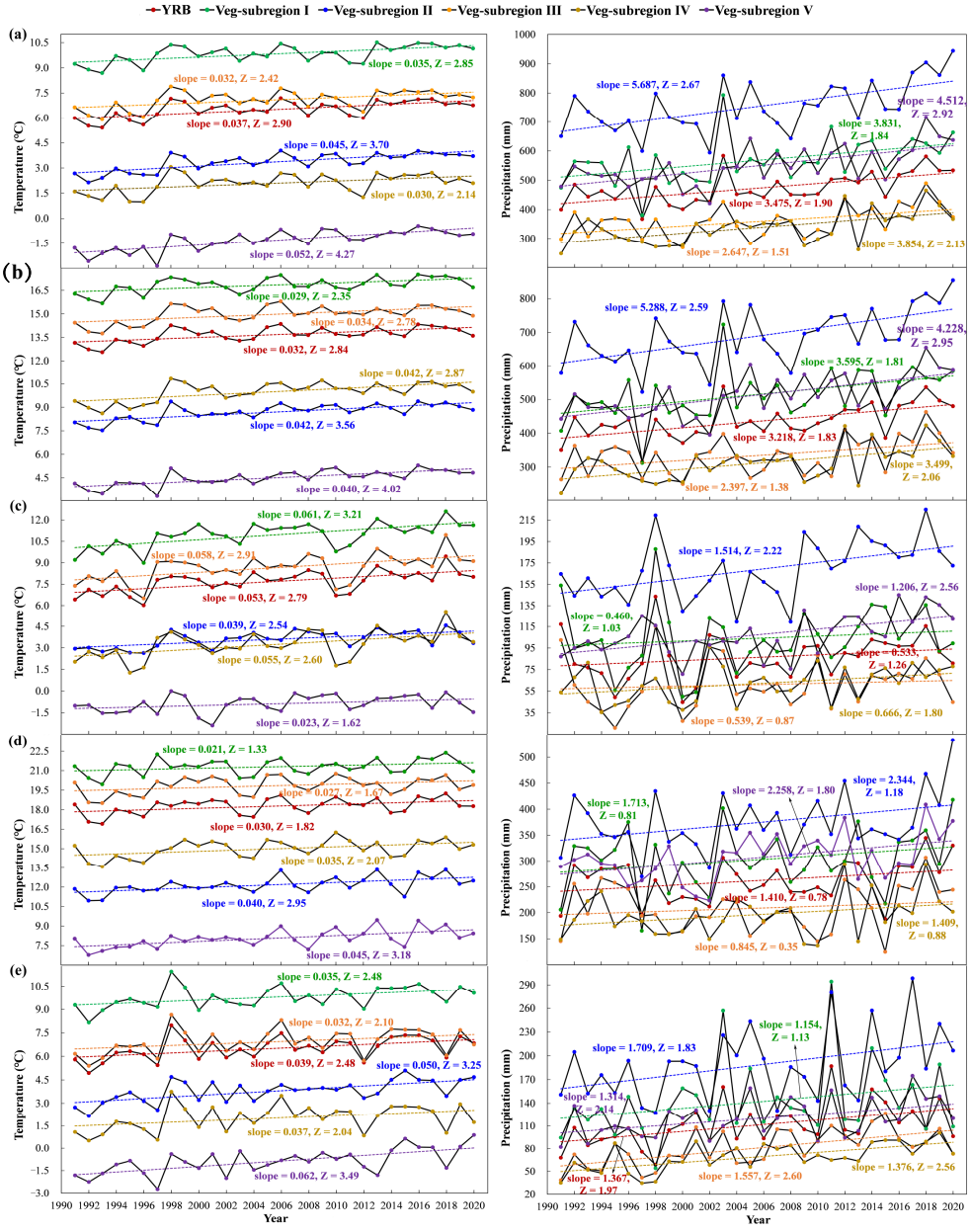

Figure 4. Variations of average temperature and precipitation in the YRB and five vegetation sub-regions during 1991–2020 for (**a**) annual, (**b**) growing season, (**c**) spring, (**d**) summer, and (**e**) autumn, respectively.

3.2.2. Spatial Distribution of Climate Change

Figure 5 shows the heterogeneous spatial trends of the climatic factors at different time scales in the YRB during 1991–2020. The annual and growing season temperatures significantly increased in more than 78.4% of the entire basin, where the highest warming rates were observed in Taiyuan Basin, Ningxia Plain, Sichuan–Tibet Plateau, and the source region of the Yellow River. In contrast, the lowest warming rates were clustered in the Hetao Plain and the central area of the middle reaches of the YRB (Figure 5a,b). The most significant increasing trend in spring temperature was observed in most areas of the Loess Plateau as well as lower reaches of the YRB, accounting for 88.4% (Figure 5c). Summer temperature showed a significant increasing trend, similar to that of the growing season, with a slight decrease (<0.1% of YRB) in some areas of the northern Loess Plateau (Figure 5d). In autumn, the temperature significantly increased in 79.6% of the study area,

which was prominently distributed in the source region of the Yellow River, Sichuan–Tibet Plateau, Qilian Mountains, Helan Mountains, and eastern YRB (Figure 5e).

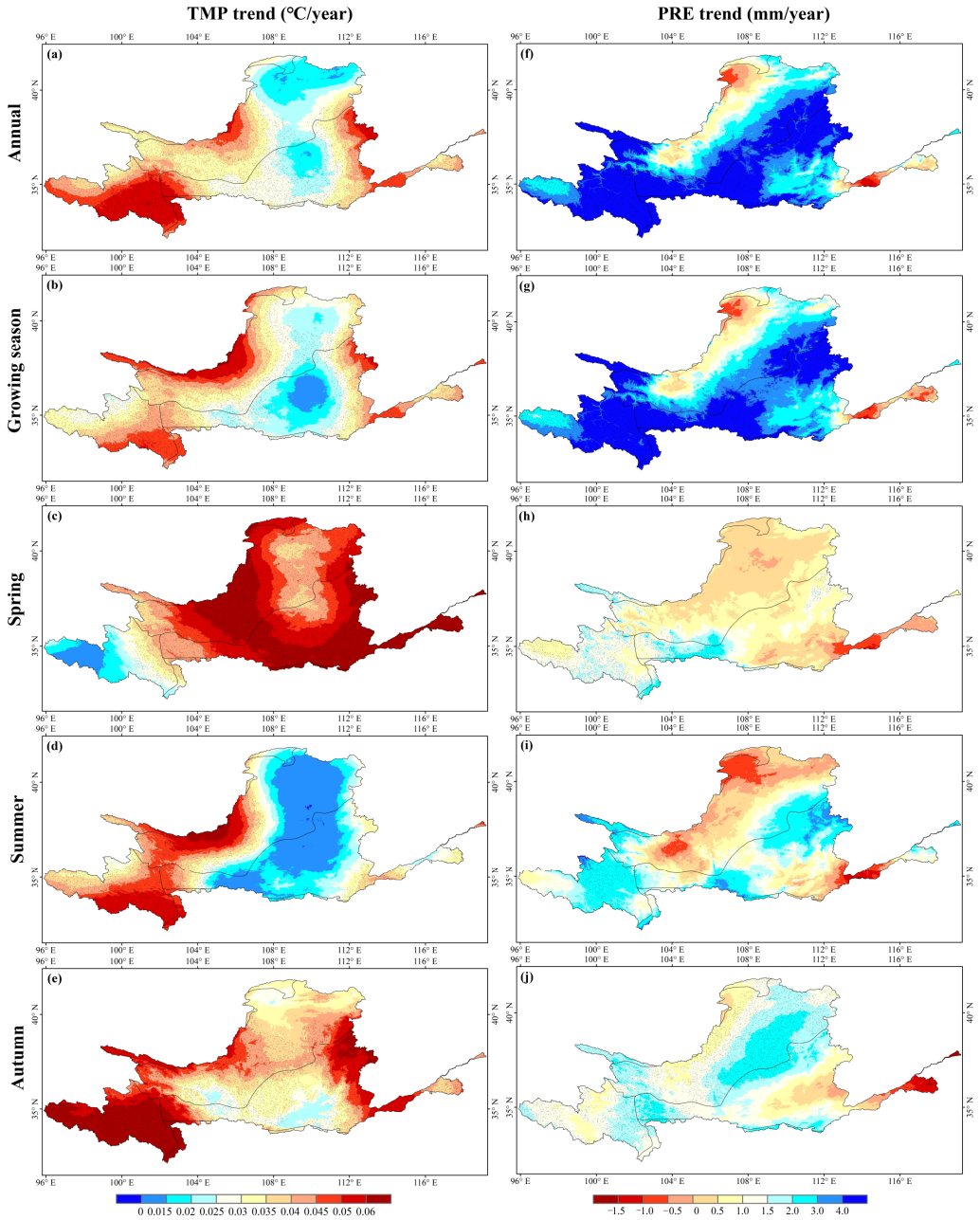

Figure 5. Spatial distribution of TMP and PRE trends in the YRB throughout 1991–2020. (**a**–**e**) The annual, growing season, spring, summer, and autumn temperature trends, respectively; (**f**–**j**) the precipitation trends for the same time scales as (**a**–**e**), respectively. Regions marked with black dots in (**a**–**j**) indicate significant trends ($p < 0.05$).

More than 96.2% of the YRB experienced a wetter trend at annual and growing season scales, with significant wetter tendencies in most areas of sub-regions I, II, and V (Figure 5f,g). However, most of the lower reaches and several northern part of the YRB (especially the areas adjacent to the Hetao Plain and Ordos Plateau) were drier. In addition, a larger area (16.7%) of the YRB showed a decreasing trend in summer precipitation, extending spatially from the Ordos Plateau to the Longzhong Plateau (Figure 5i). Pixels showing significant increasing trends in spring precipitation were mainly located in the Sichuan–Tibet Plateau, Qilian Mountains, and Taiyuan Basin (Figure 5h). Unlike other

seasons, autumn precipitation exhibited the largest area (59.1%) of significant increasing trend, primarily located in sub-regions III, IV, and V. The decreasing trend of autumn precipitation was concentrated in the lower reaches of the YRB (Figure 5j).

3.3. Effects of Climate Change on EVI Greening

To examine the relationship between vegetation greening and climatic variations in the YRB during 2000–2020, the partial correlations between EVI and TMP ($PCC_{EVI\text{-}TMP}$, precipitation is fixed) and PRE ($PCC_{EVI\text{-}PRE}$, temperature is fixed) are performed across the annual, growing season, and seasonal time ranges. In 83.56% and 66.16% of the YRB, positive correlations were observed between the annual and growing season EVI and TMP, with $PCC_{EVI\text{-}TMP}$ values of 0.199 and 0.108 ($p > 0.05$), respectively (Table 3). These positive correlations were primarily observed in regions such as the Yellow River source area, the Sichuan–Tibet Plateau, and the lower reaches of the YRB. Conversely, negative correlations were predominantly found in areas such as the Longzhong Loess Plateau, Ordos Plateau, and northern Shaanxi Loess Plateau (Figure 6a,b). 90.2% of the YRB exhibited a positive correlation between EVI and TMP in spring (Figure 6c), with the highest significant positive correlation coefficient of 0.335 observed in 38.1% of the study area. This suggests that temperature changes profoundly influenced spring vegetation greening in the YRB. Summer witnessed a larger area (46.0%) with a negative correlation between the EVI and TMP, clustered in most areas of the Loess Plateau and several regions in the lower reaches of the YRB (Figure 6d). A significant negative correlation was observed between autumn EVI and TMP in only 2.21% of the YRB, with these areas distributed in the western and northern parts of the Ordos Plateau (Figure 6e).

Table 3. Partial correlation coefficients among annual, growing season, and seasonal EVIs with TMP ($PCC_{EVI\text{-}TMP}$) and PRE ($PCC_{EVI\text{-}PRE}$) of different vegetation sub-regions in the YRB during 2000–2020.

Partial Correlation Coefficient	Sub-Region	Annual	Growing Season	Spring	Summer	Autumn
$PCC_{EVI\text{-}TMP}$	I	0.253	0.144	0.328 *	0.062	0.234
	II	0.292	0.30	0.228	0.171	0.217
	III	0.13	0.034	0.412 *	−0.05	−0.062
	IV	0.157	0.106	0.239	0.054	−0.136
	V	0.252	0.197	0.179	0.199	0.268
	YRB	0.199	0.108	0.335 *	0.038	0.103
$PCC_{EVI\text{-}PRE}$	I	0.30	0.273	0.349	0.301	−0.022
	II	0.231	0.189	0.287	0.089	0.09
	III	0.481 **	0.467 **	0.272	0.385 *	0.127
	IV	0.278	0.289	0.118	0.16	0.135
	V	0.105	0.20	0.068	0.256	−0.084
	YRB	0.343 *	0.342 *	0.263 *	0.321 *	0.038

* and ** indicate $p < 0.05$ and $p < 0.01$, respectively.

EVI was positively or significantly positively correlated with PRE in different seasons, with 88.68% annually, 89.88% in the growing season, 83.18% in spring, 89.83% in summer, and 58.35% in autumn (Figure 7b). Among them, significant positive correlations were observed in the annual, growing season, spring, and summer, with $PCC_{EVI\text{-}PRE}$ values of 0.343, 0.342, 0.263, and 0.321, respectively. These areas were concentrated in the Longzhong Loess Plateau, Ordos Plateau, and the central part of the Loess Plateau (Figure 6f–i). Negative/significant negative correlations between EVI and PRE were primarily identified in the source region of the Yellow River and in several areas of the Sichuan–Tibet Plateau, Ningxia Plain, Hetao Plain, and Guanzhong Basin, with the largest area (41.64%) in autumn. These findings indicate that vegetation coverage throughout the year, growing season, spring, and summer is sensitive to changes in precipitation.

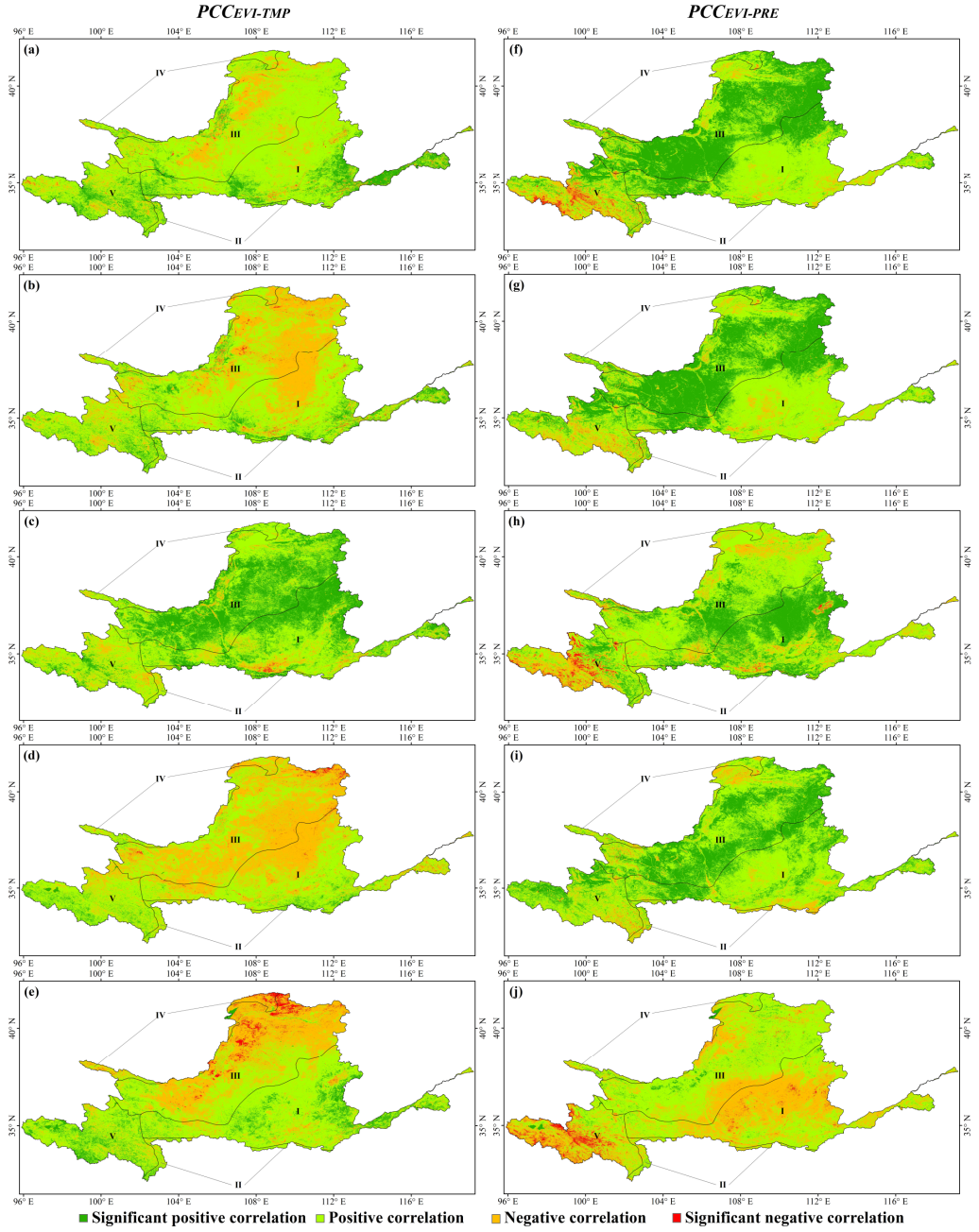

Figure 6. Partial correlations between EVI and climatic factors in the YRB during 2000–2020. (**a**–**e**) The $PCC_{EVI\text{-}TMP}$ for annual, growing season, spring, summer, and autumn, respectively; (**f**–**j**) the $PCC_{EVI\text{-}PRE}$ across five time ranges, same as (**a**–**e**).

Partial correlations of EVI with TMP and PRE were also calculated for different vegetation sub-regions. EVI was positively correlated with TMP and PRE in all sub-regions at different time scales, except in summer and autumn (Table 3). Sub-region I exhibited a significant positive correlation between EVI and spring TMP ($PCC_{EVI\text{-}TMP}$ = 0.328, $p < 0.05$), confirming that increasing temperatures in spring favored forest growth. EVI in sub-region III was positively correlated with PRE at all time scales, with the strongest significant correlation and the largest proportion in the annual ($PCC_{EVI\text{-}PRE}$ = 0.481, 66.35% of the YRB), growing season ($PCC_{EVI\text{-}PRE}$ = 0.467, 63.12% of the YRB), and summer ($PCC_{EVI\text{-}PRE}$ = 0.385, 47.95% of the YRB), suggesting that precipitation is the main limiting climatic factor for grassland growth compared to temperature. Except for summer, the EVI of sub-region V

showed the largest area of negative correlation with PRE at other time scales, especially with a proportion of 58.96% in autumn.

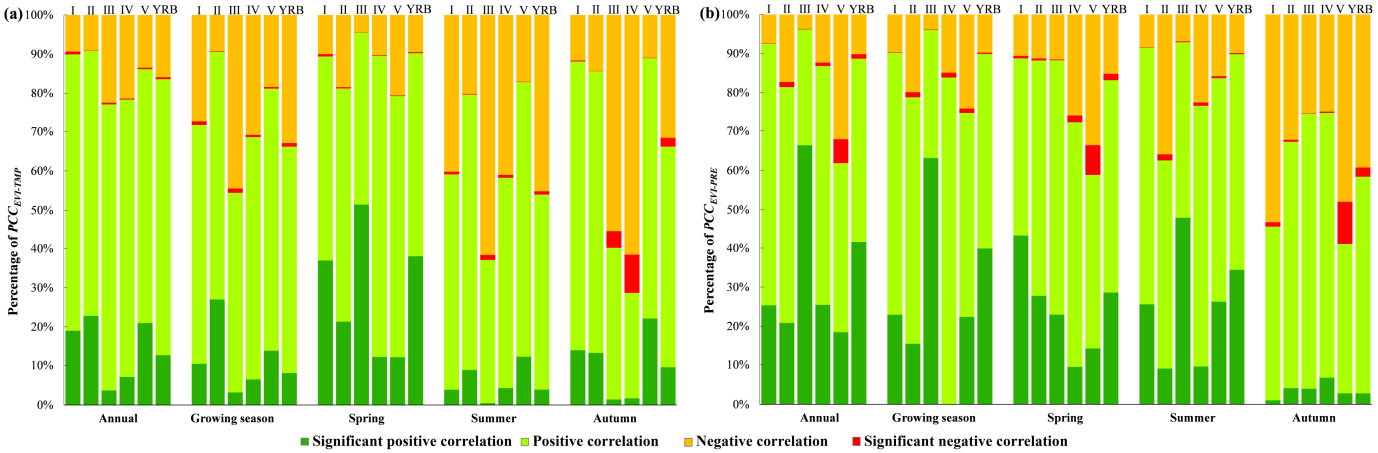

Figure 7. Area percentages of (**a**) $PCC_{EVI\text{-}TMP}$ and (**b**) $PCC_{EVI\text{-}TMP}$ for five time ranges at the basin and sub-regional scales during 2000–2020.

3.4. Spatial Residual Analysis

To distinguish the anthropogenic effect from climatic control on vegetation coverage in the YRB during 2000–2020, the growing season EVI residual trend was estimated using MLR based on TMP and PRE observations and the Theil–Sen and M–K tests. The results were classified into three categories: significant greening ($\beta > 0$, $p \leq 0.05$), significant browning ($\beta < 0$, $p \leq 0.05$), and insignificant change ($p > 0.05$). Variations in EVI can be explained by climatic factors when the residual trend is not significant; otherwise, the variations in EVI may be attributed to human activities.

Human activities positively affected the growing season EVI in 60.06% of the YRB, and these areas mainly correspond to the middle parts, especially in the Loess Plateau. In contrast, human activities negatively influenced the growing season EVI in 0.91% of the YRB, which mainly aggregated in urban areas with intense anthropogenic activity, such as Xining, Lanzhou, Yinchuan, Baotou, Huhhot, Taiyuan, Xi'an, Luoyang, and Zhengzhou (Figure 8b). Meanwhile, areas with insignificant vegetation changes occupied 39.0% of the entire basin, mainly distributed in the source region of the Yellow River, Sichuan–Tibet Plateau, Qilian Mountains, Longzhong Loess Plateau, Ningxia Plain, and Maowusu Sandy Land. Specifically, vegetation variation may be strongly attributed to climate change in these regions. According to residual analysis, human activities and climate change affected growing season vegetation in 61% and 39% of the YRB during 2000–2020, respectively (Figure 8c).

Anthropogenic and climatic impacts on vegetation coverage were further investigated in different vegetation sub-regions. The results showed that the dynamics of deciduous broad-leaved forests and grasslands were largely influenced by human activities, with significant residual trends in sub-regions I and III accounting for 77.2% and 69.6%, respectively (Figure 8d). However, both regions exhibited less than 1.0% significant browning. In contrast, changes in evergreen broad-leaved forests, deserts, and alpine vegetation were minimally affected by human activities, with insignificant changes accounting for 75.9%, 63.8%, and 89.6%, respectively. This suggests that vegetation variations in sub-regions II, IV, and V are highly related to climate change.

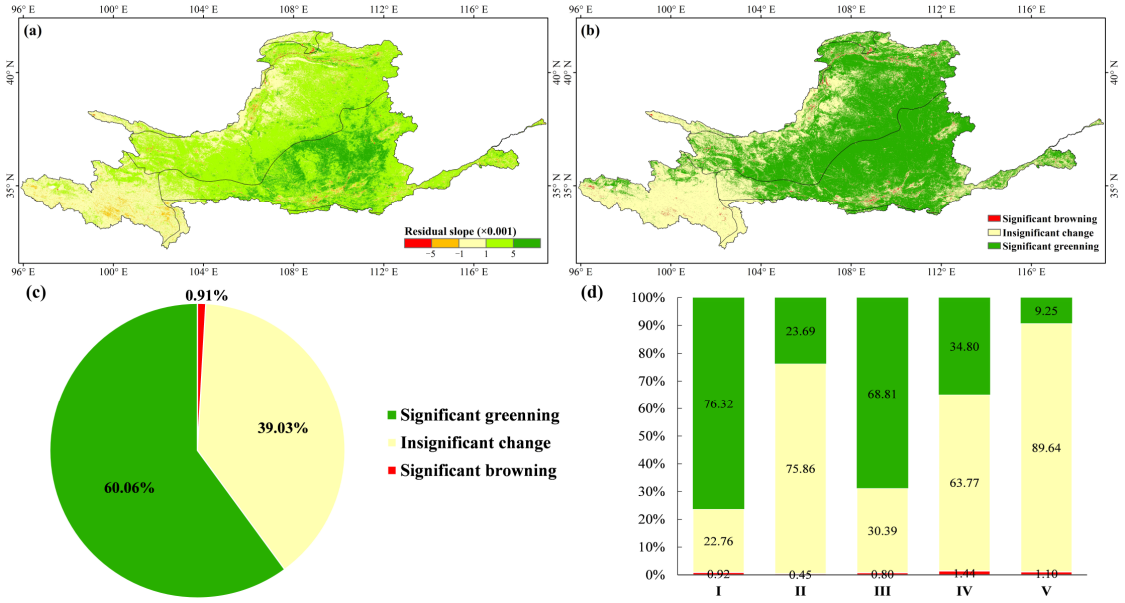

Figure 8. (**a**) Spatial distribution of residual trend in growing season EVI across the YRB during 2000–2020, (**b**) types of residual trend based on the M–K test, (**c**,**d**) percentages (%) of residual trends in the YRB and among vegetation sub-regions, respectively.

3.5. Relative Contributions of Climate Change and Human Activities to Vegetation Greening

Relative contribution analysis, calculated according to Table 1, indicated that climate change and human activities together had positive impacts on EVI greening in approximately 84.5% of the YRB during the growing season, with average relative contributions of climate change and human activities being 34.85% and 65.15%, respectively. The areas with relative contributions of climate change exceeding 60% occupied 14.6% of the entire basin experiencing vegetation greening and was mainly distributed in the source region of the Yellow River, Longzhong Loess Plateau, Sichuan–Tibet Plateau, and Maowusu Sandy Land (Figure 9a). In comparison, 67.2% of the areas where the relative contribution of human activities to greening was more than 60%, were primarily in the middle of the Loess Plateau, from the Hetao Plain to the Ordos Plateau, and then to Shaanxi Province, eastern Gansu, and southwest Shanxi in the basin (Figure 9c).

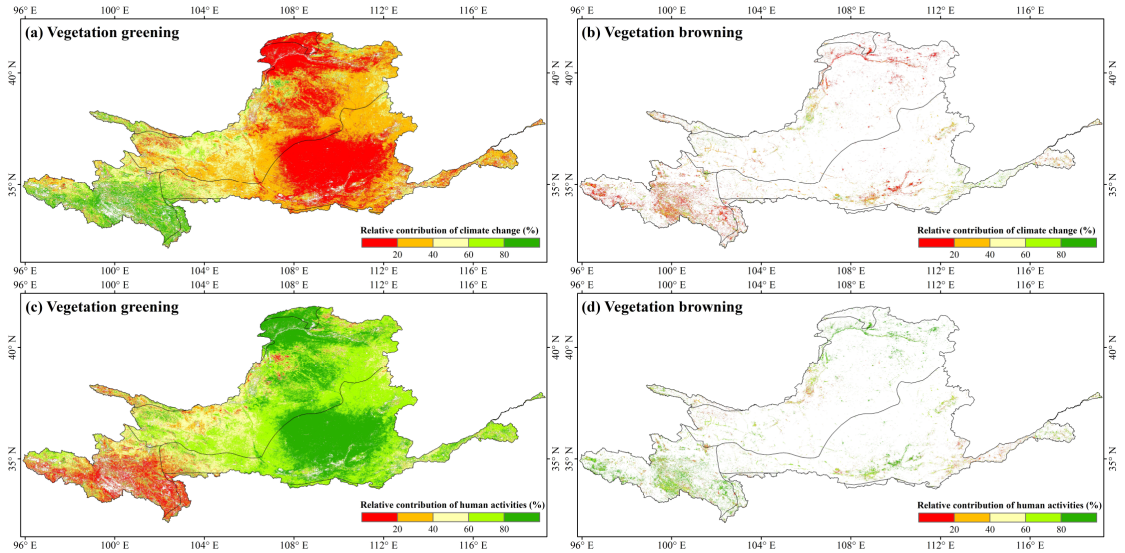

Figure 9. Relative contributions of climate change and human activities to (**a**,**c**) greening and (**b**,**d**) browning in the YRB during 2000–2020, respectively.

In areas where EVI browning was affected by climate change and human activities (3.5% of the YRB), the relative contribution of climate change was 29.70% compared to that of human activities, which was 70.3%. Contributions of climate change-induced browning exceeding 60% totaled 19.02%, which were predominantly dispersed in the eastern Sichuan–Tibet Plateau and certain areas in the lower reaches of the basin (Figure 9b), whereas human activities contributing more than 60% to browning accounted for 67.56% and were found in the southern Sichuan–Tibet Plateau and several urban areas including Xining, Lanzhou, Yinchuan, Baotou, Taiyuan, Xi'an, Luoyang, and Zhenzhou, which have high levels of anthropogenic activity (Figure 9d).

4. Discussion

4.1. Variations in Vegetation Coverage and Climatic Factors

Using the MODIS EVI dataset, this study suggested that approximately 92% of the YRB exhibited vegetation greening, of which 75% were statistically significant, with average rates of 0.0024/year and 0.0034/year derived by EVI_{AN} and EVI_{GS} during 2000–2020, respectively. This trend is consistent with previous studies on vegetation dynamics in the YRB during the past two decades, based on various MODIS NDVI datasets [24,25,33]. However, the rate of increase in EVI in this study was marginally lower than that of NDVI in previous studies, potentially due to the differences in spatial resolution and temporal scale within vegetation index datasets [34]. Compared to other NDVI datasets, such as the Global Inventory Monitoring and Modeling System (GIMMS) NDVI [35] and Systeme Probatoire d'Observation de la Terre (SPOT) Vegetation NDVI [36], this study identified a higher rate of vegetation greening during 2000–2020 than that reported in the last three decades (1982–2015). Since 2000, a notable expansion of the regions exhibiting vegetation greening in the basin has occurred, particularly in the central and eastern YRB, covering most of the Loess Plateau. This further supports the conclusions that the series of ecological rehabilitation programs implemented by the Chinese government in the Loess Plateau and other areas have considerably promoted vegetation greening since the end of the last century. However, significant browning occurred in urban areas, such as Yinchuan, Xi'an, Taiyuan, and Zhengzhou, likely due to the inhibition of urbanization [37]. Furthermore, the analysis of EVI variations in different vegetation sub-regions revealed the highest greening rate in sub-region I across all six time scales, and the significant greening trend in this region surpassed that in other sub-regions for all but spring and autumn. YRB is the primary grain production region in China, and cropland is the dominant vegetation type distributed in sub-region I [38]. This observation corroborates earlier studies, indicating a notable increase in greening trends, particularly within China's agricultural regions [10].

With respect to climate change, the YRB showed a significant warmer trend and an insignificant wetter trend (0.037 °C/year, 3.475 mm/year) during 1991–2020, and the most significant warming but smallest wetting tendency was detected in spring. The observed warming trends of the YRB at different time scales during the last 30 years were consistent with those reported in the past six decades (1961–2020), with an average warming rate of 0.30 °C per decade [39], which can be attributed to the impact of global warming. In contrast to temperature, precipitation dynamics in the YRB varied slightly during different time periods. The YRB has generally exhibited a drier trend over the past 40–60 years since 1961 [40], while a wetter trend was detected during the climatic base period of 1991–2020 [39], which is consistent with the results of the present study. To confirm the above conclusions, the monthly precipitation dataset for the YRB from 1961 to 2020 at 1 km [41], obtained from the NESSDC, was applied to investigate the precipitation variations. The YRB has experienced a drier trend over the last six decades (–0.325 mm/year, 1961–2020) but a wetter trend over the recent three decades (2.874 mm/year, 1991–2020) (Figure 10), which may be caused by the increase in annual precipitation days since 1991 [39] and the influence of increasing the intensity of extreme precipitation after 2006 [42]. This result provides further evidence of stronger unevenness in the temporal range of the hydrological cycle under global warming [43].

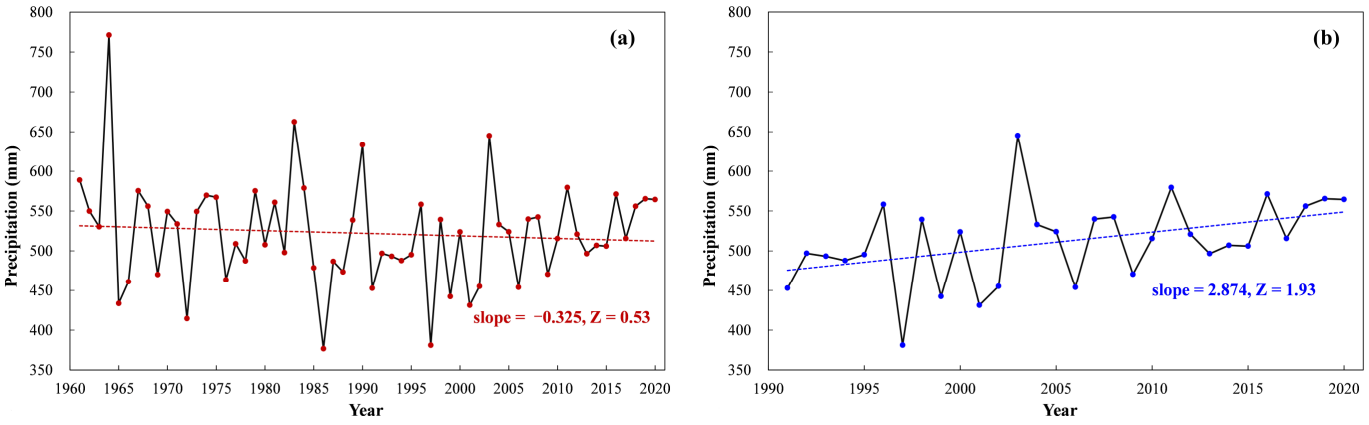

Figure 10. Precipitation changes in the YRB during (**a**) 1961–2020 and (**b**) 1991–2020, using the 1 km precipitation dataset produced by [41].

4.2. Relationship between Vegetation Greening and Climate Change

In the context of increasing precipitation and warming, vegetation in the YRB is becoming greener. However, the responses of vegetation greening to climate change varied across seasons and vegetation types. The average $PCC_{EVI\text{-}PRE}$ and $PCC_{EVI\text{-}TMP}$ in the YRB from 2000 to 2020 were 0.343 and 0.199, respectively, and precipitation was significantly positively correlated with EVI in a larger area in comparison with temperature. This result indicates that vegetation coverage in the YRB is considerably affected by precipitation. This is probably because most of the YRB is located in arid and semi-arid areas, where water resources are inherently insufficient, and precipitation is naturally the main limitation for vegetation growth [44].

However, temperature, as a controlling factor for seasonal variations in vegetation coverage, cannot be overlooked. It was discovered that in the source region of the YRB, where snowmelt is a vital supply of soil water and runoff [45], the EVI at different time ranges exhibited a positive correlation with temperature. In contrast, in some arid regions (i.e., the Loess Plateau), negative correlations between EVI and temperature were detected in the growing season, summer, and autumn. This reconfirms that vegetation responses to climate change are heterogeneous across seasons [46]. Spring EVI was significantly positively correlated with temperature and precipitation, whereas the correlation with temperature was stronger than that with precipitation. Therefore, spring EVI variations were affected by the coupling of these two climatic factors, but temperature was the dominant factor regulating vegetation coverage in spring over the YRB. Approximately 86% of the YRB exhibited vegetation greening in spring, which may be explained by warming-induced advances in the onset of vegetation photosynthetic activity and acceleration of vegetation spring green-up [47]. However, vegetation browning was more severe in spring than in summer and autumn, especially in arid areas such as the Hetao Plain; this may be attributed to rapid warming and relatively low precipitation in spring across the YRB. Climate warming might considerably enhance evapotranspiration and potentially aggregate soil moisture deficit, thus inhibiting vegetation growth in water-limited regions [48]. Generally, increased precipitation in the YRB significantly and positively affected vegetation coverage in spring and summer; however, a larger area (41.6%) of the autumn EVI was negatively correlated with precipitation, indicating that excessive precipitation in autumn may have slightly inhibited vegetation coverage.

In addition, the responses of the EVI to climatic conditions varied among different vegetation sub-regions. Similar to the relationship between EVI and temperature in the entire basin, the annual and growing season EVI were positively but not significantly correlated with temperature in all vegetation sub-regions. Spring EVI was significantly positively correlated with temperature in sub-regions I and III, probably because of the increased photosynthetic activity and lengthened growing season [49]. The EVI in sub-

region III was significantly positively correlated with precipitation at three time scales (annual, growing season, and summer), indicating that water was the dominant limiting climatic factor for grasslands. The dominant role of water conditions in grasslands has been generally confirmed in previous studies, especially in arid and semi-arid zones, such as Inner Mongolia [50] and the Loess Plateau [51].

4.3. Impacts of Climate Change and Human Activities on Vegetation Greening

Residual and relative contribution analyses revealed that the combined impacts of climate change and human activities were conducive to vegetation greening across the YRB. However, human activities had a stronger effect on greening and browning than climate change. Many studies indicated that anthropogenic activities are increasingly and profoundly influencing vegetation variations [52]. For example, a recent study by Chen et al. [10] concluded that the expansion of forests and croplands driven by human land-use management contributed to 42% and 32% of vegetation greening in China, respectively. Moreover, similar to the impact of climate change mentioned earlier, human activities affect vegetation greening both positively (ecological restoration projects) and negatively (urban expansion). Since the early 2000s, the Chinese government launched several ecological rehabilitation programs, including the Natural Forest Conservation Program and the Grain for Green Project. These initiatives have significantly contributed to regional vegetation greening [53]. Our study observed increased vegetation coverage, particularly significant greening in the center of the YRB (most areas of the Loess Plateau), where the contribution of human activities to vegetation greening exceeded 60% or even more than 80%. This finding strongly supports the hypothesis that the increase in vegetation coverage over the central YRB can be primarily attributed to policy-driven ecological projects [54]. However, increasing anthropogenic disturbances negatively impact vegetation coverage by converting land cover types from vegetated to built-up areas, a process highlighted by urban expansion and large-scale industrial activities [55]. In this study, significant browning was found in several fast-growing urban areas, most likely caused by the direct encroachment of rapid urbanization on woodlands, grasslands, and farmlands [56]. Meanwhile, the contribution of human activities to browning in the southern Sichuan–Tibet Plateau exceeded 80%, which further indicates that the construction and operation of the Qinghai–Tibet railway has resulted in the deterioration of vegetation in this region [57].

4.4. Limitations

This study has several limitations. Meteorological data from 133 ground stations were used as the climatic data to investigate the response of vegetation greening to climate change. However, owing to the small number of meteorological stations and possible errors introduced by the interpolation method, there are still uncertainties in the analysis of this relationship [58], which are difficult to solve in large-scale time-series research. In addition, except for the two key variables (namely temperature and precipitation) affecting the interaction between vegetation and climate, other climatic factors, such as evapotranspiration [38], solar radiation [59], and extreme climate [60], were not considered in the current study. The number of selected climatic factors may have been a limiting factor in this study, although no consensus exists on whether climatic variables other than temperature and precipitation presently need to be considered [27]. In addition, more detailed aspects of anthropogenic disturbances, such as land use, ecological engineering, and demographic changes, are also required to explore the influences on vegetation greening in subsequent studies.

5. Conclusions

Vegetation greening based on EVI data across the YRB and within distinct vegetation sub-regions from 2000 to 2020 and its response to climate change were investigated. The relative contributions of climate change and human activities to vegetation greening were also quantitatively assessed. Considering the increasing warming and wetter tendencies

observed over the past two decades, the YRB experienced significant vegetation greening. Greening predominantly occurred in the central and eastern regions, comprising approximately 92% of the basin, while browning was primarily confined to urban areas with high anthropogenic activity, comprising less than 6.3% of the study area. Notably, vegetation browning increased during all three seasons, especially in spring. This increase is possibly due to heightened warming and reduced precipitation in spring. In general, appropriate precipitation and temperature are the reasons for promoting vegetation greening together. Partial correlation analysis revealed that relative to temperature, precipitation emerged as the primary climatic constraint for annual and growing season vegetation growth throughout the YRB. However, the response of the EVI trends to climatic variables varied across different vegetation sub-regions and seasonal scales. For example, the EVI of cropland-dominated sub-region I exhibited a positive correlation with temperature across all time scales but a negative correlation with autumn precipitation. Conversely, the EVI in sub-region III, with predominant grassland, was positively correlated with precipitation across all time ranges and negatively correlated with summer and autumn temperatures. Overall, vegetation greening in the YRB benefited from the joint influences of climate change and human activities. However, human activities had a greater impact on vegetation dynamics across the basin than climate change. The relative contributions of human activities to vegetation greening and browning across the YRB were 65.15% and 70.30%, respectively. In particular, the ecological rehabilitation programs implemented across the Loess Plateau had positive impacts on vegetation greening, while the rapid urbanization in the basin and construction projects in the southern Sichuan–Tibet Plateau negatively affected regional greening. These findings contributed to a better understanding of spatiotemporal patterns of vegetation greening in the YRB and highlighted the importance of continued monitoring of vegetation dynamics to better adapt to climate change. Moreover, the dual impacts of human activities on vegetation greening and browning in this basin should be paid close attention, and more socioeconomic and anthropogenic datasets are required for further detailed assessment between them to guide the formulation of ecological protection and restoration management strategies and mitigate the potential adverse effects of human activities on vegetation coverage.

Author Contributions: Y.B.: conceptualization, methodology, data curation, writing—original draft, and funding acquisition. Y.Z.: methodology, formal analysis, resources, writing—review and editing. Y.L.: investigation, software, visualization, and validation. S.W.: supervision and writing—review and editing. All authors have read and agreed to the published version of the manuscript.

Funding: This work was jointly supported by the National Earth System Science Data Center (No. 2005DKA32300) and Data Center of the Chinese Academy of Sciences (WX145XQ07-11).

Data Availability Statement: The EVI data were obtained from the NASA (https://earthdata.nasa.gov/, accessed on 30 August 2023 to 12 September 2023), the DEM data were obtained from the ASTER GEDM (https://lpdaac.usgs.gov/, accessed on 21 September 2023), the meteorological data were obtained from the China Meteorological Data Service Center (http://data.cma.cn/, accessed on 21 September 2023), and the vegetation sub-region data were obtained from the NESSDC (http://www.geodata.cn/, accessed on 21 September 2023).

Conflicts of Interest: The authors declare no conflicts of interest.

References

1. Forzieri, G.; Miralles, D.G.; Ciais, P.; Alkama, R.; Ryu, Y.; Duveiller, G.; Zhang, K.; Robertson, E.; Kautz, M.; Martens, B.; et al. Increased control of vegetation on global terrestrial energy fluxes. *Nat. Clim. Chang.* **2020**, *10*, 356–362. [CrossRef]
2. Zhao, F.; Wu, Y.; Sivakumar, B.; Long, A.; Qiu, L.; Chen, J.; Wang, L.; Liu, S.; Hu, H. Climatic and hydrologic controls on net primary production in a semiarid loess watershed. *J. Hydrol.* **2019**, *568*, 803–815. [CrossRef]
3. Liu, Y.; Li, Z.; Chen, Y.; Mindje Kayumba, P.; Wang, X.; Liu, C.; Long, Y.; Sun, F. Biophysical impacts of vegetation dynamics largely contribute to climate mitigation in High Mountain Asia. *Agric. For. Meteorol.* **2022**, *327*, 109233. [CrossRef]
4. Yang, K.; Wu, H.; Qin, J.; Lin, C.; Tang, W.; Chen, Y. Recent climate changes over the Tibetan Plateau and their impacts on energy and water cycle: A review. *Glob. Planet. Chang.* **2014**, *112*, 79–91. [CrossRef]

5. Shen, M.; Piao, S.; Jeong, S.-J.; Zhou, L.; Zeng, Z.; Ciais, P.; Chen, D.; Huang, M.; Jin, C.-S.; Li, L.Z.X.; et al. Evaporative cooling over the Tibetan Plateau induced by vegetation growth. *Proc. Natl. Acad. Sci. USA* **2015**, *112*, 9299–9304. [CrossRef]
6. Zhu, Z.; Piao, S.; Myneni, R.B.; Huang, M.; Zeng, Z.; Canadell, J.G.; Ciais, P.; Sitch, S.; Friedlingstein, P.; Arneth, A.; et al. Greening of the Earth and its drivers. *Nat. Clim. Chang.* **2016**, *6*, 791–795. [CrossRef]
7. Ciais, P.; Schelhaas, M.J.; Zaehle, S.; Piao, S.L.; Cescatti, A.; Liski, J.; Luyssaert, S.; Le-Maire, G.; Schulze, E.D.; Bouriaud, O.; et al. Carbon accumulation in European forests. *Nat. Geosci.* **2008**, *1*, 425–429. [CrossRef]
8. Cheng, L.; Zhang, L.; Wang, Y.-P.; Canadell, J.G.; Chiew, F.H.S.; Beringer, J.; Li, L.; Miralles, D.G.; Piao, S.; Zhang, Y. Recent increases in terrestrial carbon uptake at little cost to the water cycle. *Nat. Commun.* **2017**, *8*, 110. [CrossRef] [PubMed]
9. Piao, S.; Wang, X.; Park, T.; Chen, C.; Lian, X.; He, Y.; Bjerke, J.W.; Chen, A.; Ciais, P.; Tømmervik, H.; et al. Characteristics, drivers and feedbacks of global greening. *Nat. Rev. Earth Environ.* **2020**, *1*, 14–27. [CrossRef]
10. Chen, C.; Park, T.; Wang, X.; Piao, S.; Xu, B.; Chaturvedi, R.K.; Fuchs, R.; Brovkin, V.; Ciais, P.; Fensholt, R.; et al. China and India lead in greening of the world through land-use management. *Nat. Sustain.* **2019**, *2*, 122–129. [CrossRef] [PubMed]
11. Piao, S.; Wang, X.; Ciais, P.; Zhu, B.; Wang, T.; Liu, J. Changes in satellite-derived vegetation growth trend in temperate and boreal Eurasia from 1982 to 2006. *Glob. Chang. Biol.* **2011**, *17*, 3228–3239. [CrossRef]
12. Ogutu, B.O.; D'Adamo, F.; Dash, J. Impact of vegetation greening on carbon and water cycle in the African Sahel-Sudano-Guinean region. *Glob. Planet. Chang.* **2021**, *202*, 103524. [CrossRef]
13. Zhou, L.; Tian, Y.; Myneni, R.B.; Ciais, P.; Saatchi, S.; Liu, Y.Y.; Piao, S.; Chen, H.; Vermote, E.F.; Song, C.; et al. Widespread decline of Congo rainforest greenness in the past decade. *Nature* **2014**, *509*, 86–90. [CrossRef] [PubMed]
14. Pan, N.; Feng, X.; Fu, B.; Wang, S.; Ji, F.; Pan, S. Increasing global vegetation browning hidden in overall vegetation greening: Insights from time-varying trends. *Remote Sens. Environ.* **2018**, *214*, 59–72. [CrossRef]
15. Qiu, B.; Ye, Z.; Chen, C.; Tang, Z.; Chen, Z.; Huang, H.; Zhao, Z.; Xu, W.; Berry, J. Dense canopies browning overshadowed by global greening dominant in sparse canopies. *Sci. Total Environ.* **2022**, *826*, 154222. [CrossRef] [PubMed]
16. Tian, F.; Fensholt, R.; Verbesselt, J.; Grogan, K.; Horion, S.; Wang, Y. Evaluating temporal consistency of long-term global NDVI datasets for trend analysis. *Remote Sens. Environ.* **2015**, *163*, 326–340. [CrossRef]
17. Le, T.S.; Harper, R.; Dell, B. Application of Remote Sensing in Detecting and Monitoring Water Stress in Forests. *Remote Sens.* **2023**, *15*, 3360. [CrossRef]
18. Norby, R.J.; Warren, J.M.; Iversen, C.M.; Medlyn, B.E.; McMurtrie, R.E. CO_2 enhancement of forest productivity constrained by limited nitrogen availability. *Proc. Natl. Acad. Sci. USA* **2010**, *107*, 19368–19373. [CrossRef]
19. Huang, M.; Piao, S.; Ciais, P.; Peñuelas, J.; Wang, X.; Keenan, T.F.; Peng, S.; Berry, J.A.; Wang, K.; Mao, J.; et al. Air temperature optima of vegetation productivity across global biomes. *Nat. Ecol. Evol.* **2019**, *3*, 772–779. [CrossRef]
20. Keenan, T.F.; Riley, W.J. Greening of the land surface in the world's cold regions consistent with recent warming. *Nat. Clim. Chang.* **2018**, *8*, 825–828. [CrossRef]
21. Doughty, C.E.; Metcalfe, D.B.; Girardin, C.A.J.; Amézquita, F.F.; Cabrera, D.G.; Huasco, W.H.; Silva-Espejo, J.E.; Araujo-Murakami, A.; da Costa, M.C.; Rocha, W.; et al. Drought impact on forest carbon dynamics and fluxes in Amazonia. *Nature* **2015**, *519*, 78–82. [CrossRef]
22. Stefanidis, S.; Rossiou, D.; Proutsos, N. Drought Severity and Trends in a Mediterranean Oak Forest. *Hydrology* **2023**, *10*, 167. [CrossRef]
23. Ge, C.; Sun, S.; Yao, R.; Sun, P.; Li, M.; Bian, Y. Long-term vegetation phenology changes and response to multi-scale meteorological drought on the Loess Plateau, China. *J. Hydrol.* **2022**, *614*, 128605. [CrossRef]
24. Tian, F.; Liu, L.-Z.; Yang, J.-H.; Wu, J.-J. Vegetation greening in more than 94% of the Yellow River Basin (YRB) region in China during the 21st century caused jointly by warming and anthropogenic activities. *Ecol. Indic.* **2021**, *125*, 107479. [CrossRef]
25. Ren, Z.; Tian, Z.; Wei, H.; Liu, Y.; Yu, Y. Spatiotemporal evolution and driving mechanisms of vegetation in the Yellow River Basin, China during 2000–2020. *Ecol. Indic.* **2022**, *138*, 108832. [CrossRef]
26. Lu, C.; Hou, M.; Liu, Z.; Li, H.; Lu, C. Variation Characteristic of NDVI and its Response to Climate Change in the Middle and Upper Reaches of Yellow River Basin, China. *IEEE J. Sel. Top. Appl. Earth Obs. Remote Sens.* **2021**, *14*, 8484–8496. [CrossRef]
27. Jian, S.; Zhang, Q.; Wang, H. Spatial–Temporal Trends in and Attribution Analysis of Vegetation Change in the Yellow River Basin, China. *Remote Sens.* **2022**, *14*, 4607. [CrossRef]
28. Lavagnini, I.; Badocco, D.; Pastore, P.; Magno, F. Theil–Sen nonparametric regression technique on univariate calibration, inverse regression and detection limits. *Talanta* **2011**, *87*, 180–188. [CrossRef] [PubMed]
29. Neeti, N.; Eastman, J.R. A Contextual Mann-Kendall Approach for the Assessment of Trend Significance in Image Time Series. *Trans. GIS* **2011**, *15*, 599–611. [CrossRef]
30. Chen, A.; He, B.; Wang, H.; Huang, L.; Zhu, Y.; Lv, A. Notable shifting in the responses of vegetation activity to climate change in China. *Phys. Chem. Earth Parts A/B/C* **2015**, *87–88*, 60–66. [CrossRef]
31. Evans, J.; Geerken, R. Discrimination between climate and human-induced dryland degradation. *J. Arid Environ.* **2004**, *57*, 535–554. [CrossRef]
32. Cao, W.; Wu, D.; Huang, L.; Pan, M.; Huhe, T. Determinizing the contributions of human activities and climate change on greening in the Beijing-Tianjin-Hebei Region, China. *Sci. Rep.* **2021**, *11*, 21201. [CrossRef] [PubMed]
33. Zhang, Z.; Liu, H.; Zuo, Q.; Yu, J.; Li, Y. Spatialtemporal change of fractional vegetation cover in the Yellow River Basin during 2000–2019. *Resour. Sci.* **2021**, *43*, 849–858. [CrossRef]

34. Jin, K.; Wang, F.; Han, J.; Shi, S.; Ding, W. Contribution of climatic change and human activities to vegetation NDVI change over China during 1982–2015. *Acta Geogr. Sin.* **2020**, *75*, 961–974.
35. Zhan, C.; Liang, C.; Zhao, L.; Jiang, S.; Niu, K.; Zhang, Y.; Cheng, L. Vegetation Dynamics and its Response to Climate Change in the Yellow River Basin, China. *Front. Environ. Sci.* **2022**, *10*, 892747. [CrossRef]
36. He, Z.; He, J. Spatio-temporal variation of vegetation cover based on SPOT-VGT in Yellow River Basin. *Ecol. Environ. Sci.* **2012**, *21*, 1655–1659. [CrossRef]
37. Miao, C.; Yang, L.; Chen, X.; Gao, Y. The vegetation cover dynamics (1982–2006) in different erosion regions of the Yellow River Basin, China. *Land Degrad. Dev.* **2012**, *23*, 62–71. [CrossRef]
38. Li, H.; He, Y.; Zhang, L.; Cao, S.; Sun, Q. Spatiotemporal changes of Gross Primary Production in the Yellow River Basin of China under the influence of climate-driven and human-activity. *Glob. Ecol. Conserv.* **2023**, *46*, e02550. [CrossRef]
39. Wang, S.; Zhao, G.; Wang, M.; Fan, X.; Wang, C. Characterisitics of climate change in the Yellow River Basin from 1961 to 2020. *Meteorol. Environ. Sci.* **2021**, *44*, 1–8.
40. Wang, Y.; Tan, D.; Han, L.; Li, D.; Wang, X.; Lu, G.; Lin, J. Review of climate change in the Yellow River Basin. *J. Desert Res.* **2021**, *41*, 235–246. [CrossRef]
41. Peng, S.; Ding, Y.; Liu, W.; Li, Z. 1 km monthly temperature and precipitation dataset for China from 1901 to 2017. *Earth Syst. Sci. Data* **2019**, *11*, 1931–1946. [CrossRef]
42. Ma, J.; Gao, Y. Analysis of annual precipitation and extreme precipitation change in the upper Yellow River Basin in recent 50 years. *Plateau Meteorol.* **2019**, *38*, 124–135.
43. Zhang, W.; Furtado, K.; Wu, P.; Zhou, T.; Chadwick, R.; Marzin, C.; Rostron, J.; Sexton, D. Increasing precipitation variability on daily-to-multiyear time scales in a warmer world. *Sci. Adv.* **2021**, *7*, eabf8021. [CrossRef] [PubMed]
44. Zhan, Y.; Ma, C.; Yan, Y.; Zhu, J.; Ji, Y.; Ma, C.; Luo, Y. Spatial differentiation characteristics of vegetation greening rates and climate attribution in China's arid and semi-arid regions. *Glob. Ecol. Conserv.* **2023**, *46*, e02563. [CrossRef]
45. Li, Z.; Zhang, S.; Meng, X.; Lyu, S.; Yang, X.; Ao, Y.; Ma, D.; Shang, L.; Shu, L.; Chang, Y. Effect of snow cover on water and heat transfer in alpine meadows in the source region of Yellow River. *Sci. Total Environ.* **2023**, *859*, 160205. [CrossRef] [PubMed]
46. Kong, D.; Zhang, Q.; Singh, V.P.; Shi, P. Seasonal vegetation response to climate change in the Northern Hemisphere (1982–2013). *Glob. Planet. Chang.* **2017**, *148*, 1–8. [CrossRef]
47. Garonna, I.; de Jong, R.; Schaepman, M.E. Variability and evolution of global land surface phenology over the past three decades (1982–2012). *Glob. Chang. Biol.* **2016**, *22*, 1456–1468. [CrossRef]
48. Xu, S.; Yu, Z.; Yang, C.; Ji, X.; Zhang, K. Trends in evapotranspiration and their responses to climate change and vegetation greening over the upper reaches of the Yellow River Basin. *Agric. For. Meteorol.* **2018**, *263*, 118–129. [CrossRef]
49. Ren, S.; Chen, X.; Pan, C. Temperature-precipitation background affects spatial heterogeneity of spring phenology responses to climate change in northern grasslands (30° N–55° N). *Agric. For. Meteorol.* **2022**, *315*, 108816. [CrossRef]
50. Su, R.; Yu, T.; Dayananda, B.; Bu, R.; Su, J.; Fan, Q. Impact of climate change on primary production of Inner Mongolian grasslands. *Glob. Ecol. Conserv.* **2020**, *22*, e00928. [CrossRef]
51. Zhang, X.; Zhao, W.; Liu, Y.; Fang, X.; Feng, Q. The relationships between grasslands and soil moisture on the Loess Plateau of China: A review. *CATENA* **2016**, *145*, 56–67. [CrossRef]
52. Lü, Y.; Zhang, L.; Feng, X.; Zeng, Y.; Fu, B.; Yao, X.; Li, J.; Wu, B. Recent ecological transitions in China: Greening, browning and influential factors. *Sci. Rep.* **2015**, *5*, 8732. [CrossRef] [PubMed]
53. Li, J.; Peng, S.; Li, Z. Detecting and attributing vegetation changes on China's Loess Plateau. *Agric. For. Meteorol.* **2017**, *247*, 260–270. [CrossRef]
54. Qian, C.; Shao, L.; Hou, X.; Zhang, B.; Chen, W.; Xia, X. Detection and attribution of vegetation greening trend across distinct local landscapes under China's Grain to Green Program: A case study in Shaanxi Province. *CATENA* **2019**, *183*, 104182. [CrossRef]
55. Yao, R.; Cao, J.; Wang, L.; Zhang, W.; Wu, X. Urbanization effects on vegetation cover in major African cities during 2001–2017. *Int. J. Appl. Earth Obs. Geoinf.* **2019**, *75*, 44–53. [CrossRef]
56. Bren d'Amour, C.; Reitsma, F.; Baiocchi, G.; Barthel, S.; Güneralp, B.; Erb, K.-H.; Haberl, H.; Creutzig, F.; Seto, K.C. Future urban land expansion and implications for global croplands. *Proc. Natl. Acad. Sci. USA* **2017**, *114*, 8939–8944. [CrossRef]
57. Luo, L.; Ma, W.; Zhuang, Y.; Zhang, Y.; Yi, S.; Xu, J.; Long, Y.; Ma, D.; Zhang, Z. The impacts of climate change and human activities on alpine vegetation and permafrost in the Qinghai-Tibet Engineering Corridor. *Ecol. Indic.* **2018**, *93*, 24–35. [CrossRef]
58. Shen, X.; Liu, B.; Henderson, M.; Wang, L.; Jiang, M.; Lu, X. Vegetation Greening, Extended Growing Seasons, and Temperature Feedbacks in Warming Temperate Grasslands of China. *J. Clim.* **2022**, *35*, 5103–5117. [CrossRef]
59. Ren, H.; Wen, Z.; Liu, Y.; Lin, Z.; Han, P.; Shi, H.; Wang, Z.; Su, T. Vegetation response to changes in climate across different climate zones in China. *Ecol. Indic.* **2023**, *155*, 110932. [CrossRef]
60. Liu, J.; Wei, L.; Zheng, Z.; Du, J. Vegetation cover change and its response to climate extremes in the Yellow River Basin. *Sci. Total Environ.* **2023**, *905*, 167366. [CrossRef]